

Anomalous Hall effect of facing-target sputtered ferrimagnetic Mn_4N epitaxial films with perpendicular magnetic anisotropy

Zeyu Zhang(张泽宇), Qiang Zhang(张强), and Wenbo Mi(米文博)
Citation: Chin. Phys. B, 2022, 31 (**4**): 047305. DOI: 10.1088/1674-1056/ac2b90
Journal homepage: http://cpb.iphy.ac.cn; http://iopscience.iop.org/cpb

What follows is a list of articles you may be interested in

Evaluation of threading dislocation density of strained Ge epitaxial layer by high resolution x-ray diffraction

Yuan-Hao Miao(苗渊浩), Hui-Yong Hu(胡辉勇), Xin Li(李鑫), Jian-Jun Song(宋建军), Rong-Xi Xuan(宣荣喜), He-Ming Zhang(张鹤鸣)
Chin. Phys. B, 2017, 26 (**12**): 127309. DOI: 10.1088/1674-1056/26/12/127309

Quantum anomalous Hall effect in real materials

Jiayong Zhang(张加永), Bao Zhao(赵宝), Tong Zhou(周通), Zhongqin Yang(杨中芹)
Chin. Phys. B, 2016, 25 (**11**): 117308. DOI: 10.1088/1674-1056/25/11/117308

AlO_x/LiF composite protection layer for Cr-doped $(Bi, Sb)_2Te_3$ quantum anomalous Hall films

Yunbo Ou(欧云波), Yang Feng(冯洋), Xiao Feng(冯硝), Zhenqi Hao(郝镇齐), Liguo Zhang(张立果), Chang Liu(刘畅), Yayu Wang(王亚愚), Ke He(何珂), Xucun Ma(马旭村), Qikun Xue(薛其坤)
Chin. Phys. B, 2016, 25 (**8**): 087307. DOI: 10.1088/1674-1056/25/8/087307

Silicene on substrates: A theoretical perspective

Zhong Hong-Xia, Quhe Ru-Ge, Wang Yang-Yang, Shi Jun-Jie, Lü Jin
Chin. Phys. B, 2015, 24 (**8**): 087308. DOI: 10.1088/1674-1056/24/8/087308

From magnetically doped topological insulator to the quantum anomalous Hall effect

He Ke, Ma Xu-Cun, Chen Xi, Lü Li, Wang Ya-Yu, Xue Qi-Kun
Chin. Phys. B, 2013, 22 (**6**): 067305. DOI: 10.1088/1674-1056/22/6/067305

Anomalous Hall effect of facing-target sputtered ferrimagnetic Mn_4N epitaxial films with perpendicular magnetic anisotropy

Zeyu Zhang(张泽宇)[1], Qiang Zhang(张强)[2], and Wenbo Mi(米文博)[1,†]

[1] *Tianjin Key Laboratory of Low Dimensional Materials Physics and Preparation Technology, School of Science, Tianjin University, Tianjin* 300354, *China*

[2] *Core Technology Platforms, New York University Abu Dhabi, P.O. Box* 129188, *Abu Dhabi, United Arab Emirates*

(Received 20 August 2021; revised manuscript received 13 September 2021; accepted manuscript online 30 September 2021)

Epitaxial Mn_4N films with different thicknesses were fabricated by facing-target reactive sputtering and their anomalous Hall effect (AHE) is investigated systematically. The Hall resistivity shows a reversed magnetic hysteresis loop with the magnetic field. The magnitude of the anomalous Hall resistivity sharply decreases with decreasing temperature from 300 K to 150 K. The AHE scaling law in Mn_4N films is influenced by the temperature-dependent magnetization, carrier concentration and interfacial scattering. Different scaling laws are used to distinguish the various contributions of AHE mechanisms. The scaling exponent $\gamma > 2$ for the conventional scaling in Mn_4N films could be attributed to the residual resistivity ρ_{xx0}. The longitudinal conductivity σ_{xx} falls into the dirty regime. The scaling of $\rho_{AH} = \alpha\rho_{xx0} + b\rho_{xx}^n$ is used to separate out the temperature-independent ρ_{xx0} from extrinsic contribution. Moreover, the relationship between ρ_{AH} and ρ_{xx} is fitted by the proper scaling to clarify the contributions from extrinsic and intrinsic mechanisms of AHE, which demonstrates that the dominant mechanism of AHE in the Mn_4N films can be ascribed to the competition between skew scattering, side jump and the intrinsic mechanisms.

Keywords: Mn_4N, epitaxial film, anomalous Hall effect, scaling law

PACS: 73.61.At, 75.47.Np, 75.50.Gg, 72.10.Di **DOI:** 10.1088/1674-1056/ac2b90

1. Introduction

The electrical control of spin in magnetic materials and devices plays an important role in the spintronics applications. The current-induced magnetization reversal or domain wall motion could be applied in magnetic recording, nonvolatile memory and energy-efficient devices.[1–3] The discovery of spin–orbit torque (SOT) has opened a series of opportunities to manipulate magnetization efficiently.[4,5] Recently, transition metal nitrides have gained much interest due to their excellent magnetic, electronic and chemical properties.[6,7] Mn_4N is a typical transition metal nitride with the antiperovskite structure.[8,9] In particular, Mn_4N shows ferrimagnetism with a Curie temperature of 745 K,[6] while other Mn–N compounds are antiferromagnetic.[10,11] Compared to Fe_4N that also has antiperovskite structure, the high Curie temperature, high saturation magnetization and high spin polarization of Fe_4N make it a potential candidate for magnetic recording and logical processing devices.[12,13] However, the in-plane magnetic anisotropy limits applications of Fe_4N. Materials with low saturation magnetization could reduce the critical switching current density for SOT reversal of magnetization.[14] Therefore, the perpendicular magnetic anisotropy (PMA) and low saturation magnetization in Mn_4N films reveal the potential of Mn_4N in spin-torque applications.[15,16] Moreover, the reports about the high domain wall mobility in Mn_4N films also confirmed that Mn_4N is a promising candidate for spintronics applications.[17–19]

The anomalous Hall effect (AHE) could be regarded as a useful tool to control spin-polarized currents and to characterize the magnetization.[20,21] Therefore, studying the spin-dependent transport properties of magnetic materials is beneficial to design of functional devices in spintronics.[22,23] In order to distinguish various contributions to the AHE, the conventional scaling law of $\rho_{AH} \propto \rho_{xx}^{\gamma}$ was proposed,[20] where ρ_{AH} is anomalous Hall resistivity and ρ_{xx} is longitudinal resistivity. The skew scattering mechanism leads to $\gamma = 1$,[24] while the side jump mechanism and intrinsic mechanisms leads to $\gamma = 2$.[25,26] The magnitude of ρ_{xx} in Mn_4N film is about 10^2 μΩ·cm, which lies in the region of Fe (10 μΩ·cm) and Fe_3O_4 (10^4 μΩ·cm). The AHEs of Fe and Fe_3O_4 films have been investigated and they are in good agreement with the theory.[27,28] Although the AHE in Mn_4N films has been investigated in recent years,[29–32] the origin of AHE in Mn_4N films fabricated by reactive sputtering remains controversial. The clarification between the different contributions of the AHE in Mn_4N films is of fundamental importance for applications of Mn_4N.

In this work, the AHE of epitaxial Mn_4N films with different thicknesses fabricated by reactive facing-target sputtering is investigated in details. Different scaling laws are used

†Corresponding author. E-mail: miwenbo@tju.edu.cn

© 2022 Chinese Physical Society and IOP Publishing Ltd

to clarify the various contributions of AHE mechanisms. The effects of film thickness, magnetization and carrier concentration on the AHE scaling in Mn_4N films are studied. The scaling exponent $\gamma > 2$ is found in Mn_4N films with different thicknesses by the conventional scaling of $\rho_{AH} \propto \rho_{xx}^{\gamma}$, which could be ascribed to the influence of residual resistivity. Different contributions from extrinsic and intrinsic mechanisms to AHE of Mn_4N films are also investigated.

2. Experimental details

Mn_4N films with different thicknesses ($t = 4.7$, 7.8, 11.0, 15.8, 23.6, 31.5, 47.3, and 78.8 nm) were fabricated on MgO (001) substrates by the direct-current (DC) facing-target reactive sputtering from a pair of Mn targets (99.95%) with substrate temperature 505 °C. The gas mixture of Ar (99.999%) and N_2 (99.999%) was introduced to the chamber and the pressure was kept at 1.0 Pa during the deposition. The sputtering power on the targets was 61 W. The surface morphology was analyzed by atomic force microscopy (AFM). The film thickness was determined using a Dektak 6M surface profiler and confirmed by transmission electron microscopy (TEM). The deposition rate was about 7.9 nm/min. The microstructures of the films were analyzed by x-ray diffraction (XRD) with Cu K_α radiation ($\lambda = 1.5406$ Å) and high-resolution TEM (HR-TEM). The magnetic properties were measured by a Quantum Design magnetic properties measurement system. The electronic transport properties were measured by a Quantum Design physical property measurement system. The Hall resistivity ρ_{xy} was measured in a magnetic field applied perpendicular to the film plane range from −70 kOe to +70 kOe. In order to eliminate the contribution of ρ_{xx}, the real $\rho_{xy}(H)$ was obtained by subtracting the ρ_{xy} (+70 kOe → −70 kOe) from ρ_{xy} (−70 kOe → +70 kOe) to remove the longitudinal resistivity component, which is found to be constant as a function of the magnetic field.

3. Results and discussion

To show the thickness dependence of surface roughness, the surface morphologies of the Mn_4N films were obtained by AFM. Figure 1(a) displays the AFM images with scan range of 5 μm × 5 μm for 7.8–47.3 nm-thick Mn_4N films. The average surface roughness R_a is defined as the arithmetic average deviation from the mean line within the assessment length.[33] The R_a values for the 7.8, 15.8, 23.6 and 47.3 nm-thick Mn_4N films are 0.293, 0.276, 0.277 and 0.443 nm, respectively, which show relatively smooth surfaces of films.

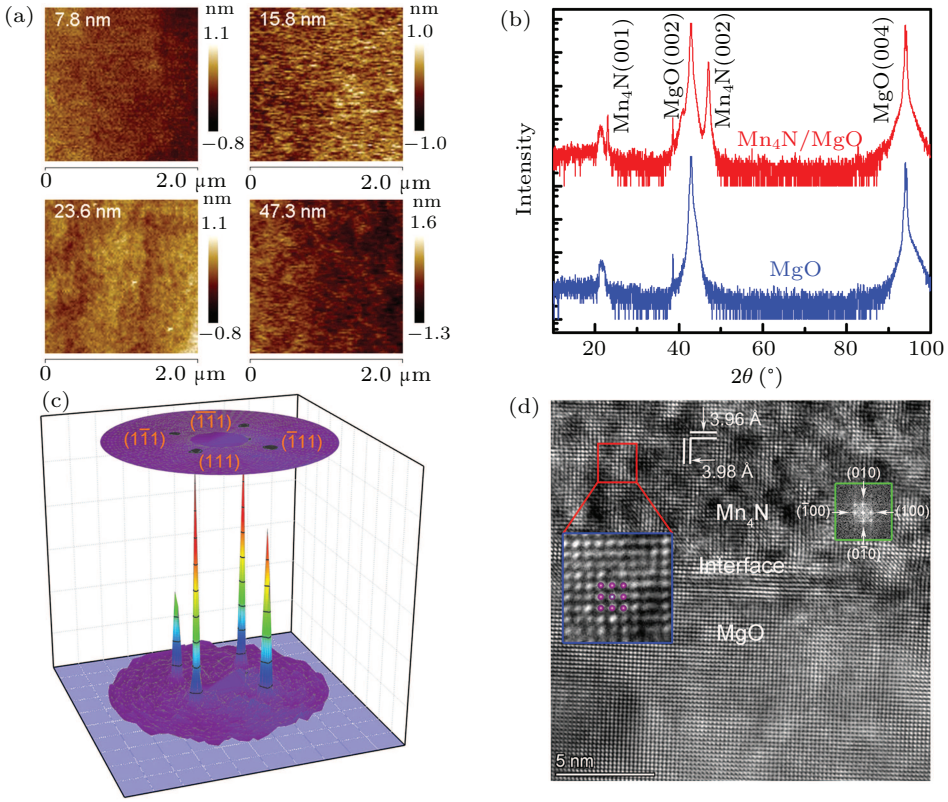


Fig. 1. (a) AFM images of the 7.8, 15.8, 23.6 and 78.8 nm-thick Mn_4N films. (b) XRD θ–2θ pattern of the 78.8 nm-thick Mn_4N film on the MgO (001) substrate. The XRD pattern of the MgO (001) substrate is shown as a reference. (c) XRD pole figure of the 78.8 nm-thick Mn_4N film. (d) Cross-sectional HR-TEM image of the Mn_4N/MgO interface of the 78.8 nm-thick Mn_4N film. The inset in the green square is the corresponding FFT diffraction image of the area in the red square and The inset in the blue square is the inverse FFT image of the FFT image.

Figure 1(b) shows the XRD patterns of the 78.8 nm-thick Mn_4N film and the MgO (001) substrate. Only the diffraction peaks (00l) from the Mn_4N film are observed, which suggests that the films grow with a preferred (001) orientation. Based on Bragg's law, the calculated lattice constant of the Mn_4N films is 3.93 Å, which is quite close to 3.87 Å of the Mn_4N films prepared by molecular beam epitaxy.[16] Figure 1(c) shows the XRD pole figure of the Mn_4N film on the MgO (001) substrate. The pole figure was collected at $2\theta = 40.365°$ and α from 20° to 90°. At $\alpha = 35.3°$, there is no peak from the MgO substrate and only the Mn_4N (111) peak appears. As seen in Fig. 1(c), the strong diffraction peaks (111) indicate the film to be epitaxial.

Figure 1(d) shows the HR-TEM image of the interface between the 78.8 nm-thick Mn_4N film and the MgO substrate. The inset in the green square is the fast Fourier transform (FFT) diffraction image of the area labeled by red square. The FFT diffraction image also indicates the epitaxial growth of the Mn_4N film, which is consistent with the XRD results. The inset in the blue square is the inverse FFT image of the FFT image, where one can clearly observe the orderly arranged Mn and N atoms, indicating a high-quality growth of the Mn_4N film. Purple (Mn atoms) and white (N atom) dots were added to show different atoms. The magnified view of the Mn_4N layer indicates the d-spacing of the film to be about 3.98 Å for (100) plane and 3.96 Å for (001) plane. The (001) d-spacing is larger than the XRD results of 3.93 Å, which is attributed to the influence of Mn_4N/MgO interface on the structure of the Mn_4N film.

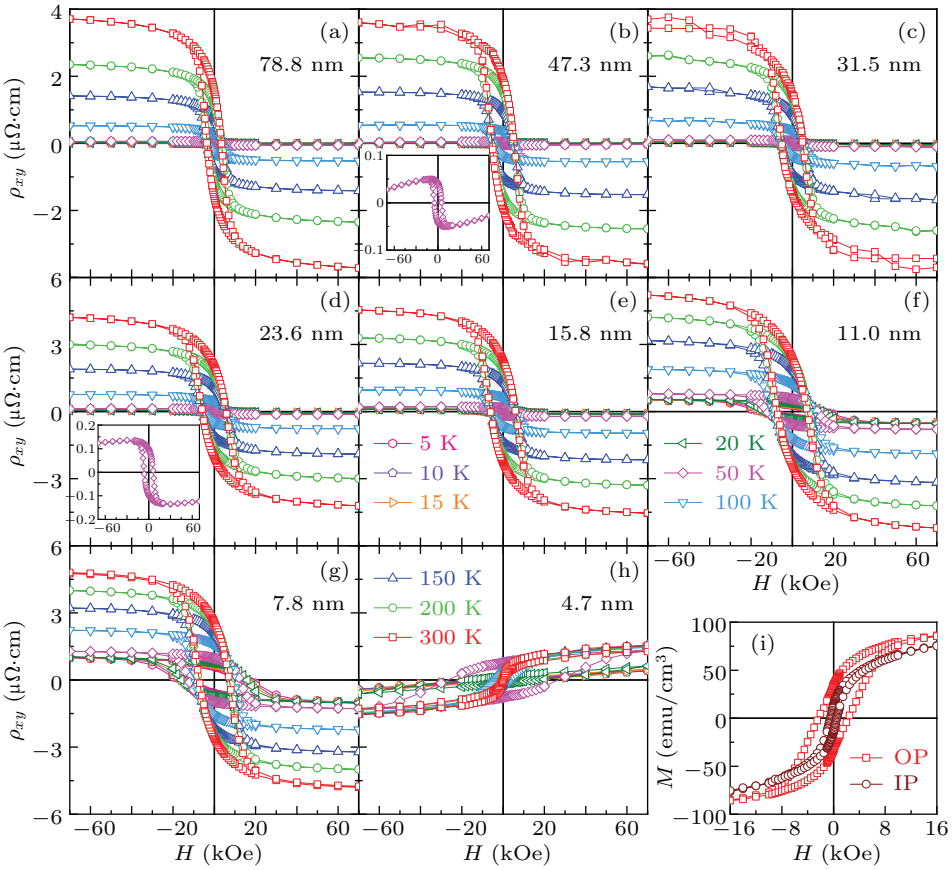


Fig. 2. Magnetic field-dependent Hall resistivity $\rho_{xy}(H)$ of the (a) 78.8, (b) 47.3, (c) 31.5, (d) 23.6, (e) 15.8, (f) 11.0, (g) 7.8 and (h) 4.7 nm-thick Mn_4N films at different temperatures. (i) M–H curves of the 78.8 nm-thick Mn_4N film measured along the in-plane and out-of-plane applied magnetic field at 300 K.

Electronic transport properties of the Mn_4N films were investigated in the temperature range of 5–300 K. The Hall-bar shaped samples were used for measuring the Hall resistivity ρ_{xy} of Mn_4N films with the thickness of 4.7–78.8 nm. Figures 2(a)–2(h) show the ρ_{xy}–H curves of Mn_4N films with different thicknesses at 5–300 K. Figure 2(i) shows the M–H curves of the 78.8-nm-thick Mn_4N film measured along the in-plane and out-of-plane applied magnetic field at 300 K. The hysteresis loops are clearly open in the magnetic field perpendicular to the films, which indicates the PMA of Mn_4N films. The hysteresis loops of Hall resistivity show the similar behavior with that of field-dependent magnetization, which is different from the Hall resistivity of Fe_4N.[34] The linear field dependence of Hall resistivity in the high-field regions

originates from the ordinary Hall effect, which is caused by Lorentz force.[35] The Hall resistivity including ordinary Hall resistivity (ρ_{OH}) and anomalous Hall resistivity (ρ_{AH}) can be expressed as $\rho_{xy} = \rho_{OH} + \rho_{AH} = R_0 H + R_s 4\pi M$, where R_0 and R_s are ordinary and anomalous Hall coefficients, respectively, M is the magnetization perpendicular to the film plane. The ρ_{OH} was proportional to the applied magnetic field, and its sign follows the type of the charge carriers. The anomalous Hall resistivity ρ_{AH} is obtained by subtracting the ordinary Hall component $R_0 H$ from Hall resistivity by linearly fitting the high-field regions of the ρ_{xy}–H curves, where the slope and y-axis intercept corresponds to R_0 and ρ_{AH}, respectively. The insets of Figs. 2(b) and 2(d) display the ρ_{xy}–H curves at 50 K, which shows a positive slope in high-field regions. The variation of slope implies the sign reversal of carrier concentration. The temperature-dependent carrier type transition indicates the change of electronic filling status and the shift of Fermi energy level in a topological structure.[36] The low temperature anomaly of the Hall resistivity is presumed to be caused by the tetragonal crystal field effect due to the structure distortion.[31] Note that the ρ_{xy}–H curves of the 4.7 nm-thick Mn_4N film are significantly different from other curves. The hysteresis behavior of ρ_{xy} has disappeared and the sign reversal of R_0 from negative to positive. The sign reversal of AHE is related to the change of band structure in the ultrathin films.[37] In addition, the sign reversal has also been observed in other materials such as $(Bi_{1-x}Mn_x)_2Se_3$ films.[38,39]

Figure 3(a) displays the temperature-dependent ρ_{AH} of Mn_4N films with 7.8–78.8 nm thicknesses. The ρ_{AH} increases sharply with the increasing temperature at 100–300 K. Below 100 K, the ρ_{AH} shows weak temperature dependence. The ρ_{AH} of the 31.5 nm-thick Mn_4N film is 2.698 μΩ·cm at 300 K, which is comparable to the value (2.8 μΩ·cm) for the 35 nm-thick Mn_4N film fabricated by pulsed laser deposition[32] and also comparable with the typical PMA materials such as $L1_0$-type FePt film (1.7 μΩ·cm) and amorphous Tb_xCo_{1-x} (2 μΩ·cm).[40,41] The value of ρ_{AH} at room temperature is lower than that of the Fe_4N film (14.15 μΩ·cm) due to the higher conductivity.[34] In Fig. 3(b), R_0 is negative, suggesting that electrons dominate transport properties. The R_s determined by the $\rho_{AH}/4\pi M_s$ is displayed in Fig. 3(c), which decreases with decreasing temperature monotonically and approaches almost zero at low temperature. Moreover, the carrier mobility μ defined by $\mu = R_0/\rho_{xx}$ is displayed in Fig. 3(d). The μ of Mn_4N films with different thicknesses increases with the increasing temperature from 5–50 K, and decreases in the temperature range from 50 to 300 K. The magnitude of μ about 10^2 $cm^2/(V{\cdot}s)$ in Mn_4N is one order larger than that in Mn_2PtSn films (30 $cm^2/(V{\cdot}s)$),[42] which is consistent with the high conductivity of Mn_4N films.

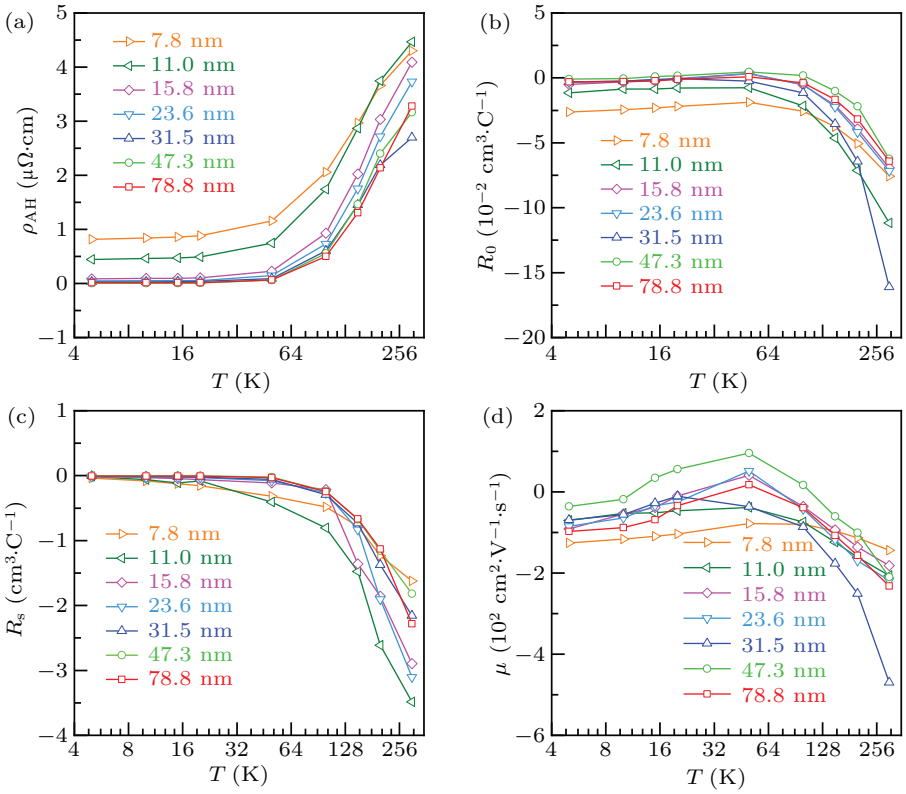


Fig. 3. Temperature-dependent (a) ρ_{AH}, (b) R_0, (c) R_s and (d) μ of Mn_4N films with different thicknesses on MgO substrates.

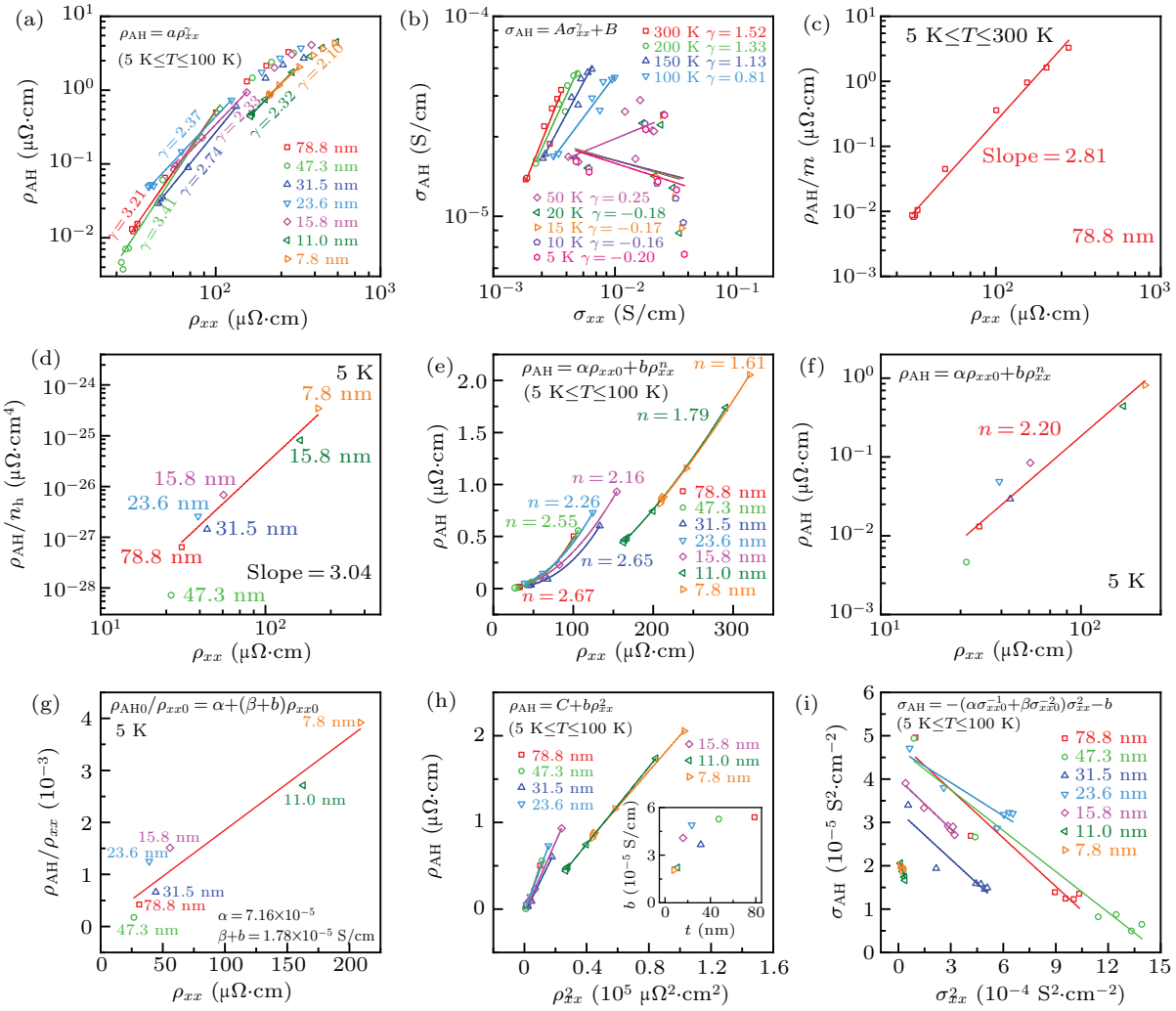


Fig. 4. (a) Relation of logρ_{AH} vs. logρ_{xx} of Mn_4N films with different thicknesses below 100 K, based on the conventional scaling of $\rho_{AH}=a\rho_{xx}^{\gamma}$. (b) Plots of σ_{AH} vs. σ_{xx} at different measured temperatures with the fitting lines by $\sigma_{AH}=A\sigma_{xx}^{\gamma}+B$. (c) Plots of log$\rho_{AH}/m$ vs. logρ_{xx} for the 78.8 nm-thick Mn_4N film at 5–300 K. (d) Plots of ρ_{AH}/n_h vs. ρ_{xx} in log-log scale of the Mn_4N films with different thicknesses at 5 K. (e) Plots of ρ_{AH} vs. ρ_{xx} for Mn_4N films with different thicknesses below 100 K by the scaling of $\rho_{AH}=\alpha\rho_{xx0}+b\rho_{xx}^{n}$. (f) Plots of log$\rho_{AH}$ vs. logρ_{xx} for Mn_4N films with different thicknesses at 5 K. (g) Plots of ρ_{AH}/ρ_{xx} vs ρ_{xx} at 5 K, with ρ_{xx0} being the longitudinal resistivity at 5 K, the red line being the linear fit by $\rho_{AH0}/\rho_{xx0}=\alpha+(\beta+b)\rho_{xx0}$. The intercept is parameter α and the slope is $(\beta+b)$. (h) Plots of ρ_{AH} vs. ρ_{xx}^{2}. Inset is the intrinsic contribution b obtained by the slope of fitting lines in (h). (i) The relation between σ_{AH} and σ_{xx}^{2} of the Mn_4N films with different thicknesses, satisfying the $\sigma_{AH}=-(\alpha\sigma_{xx0}^{-1}+\beta\sigma_{xx0}^{-2})\sigma_{xx}^{2}-b$.

The origin of the AHE mechanism could be characterized by exponential factor γ in the conventional scaling of $\rho_{AH}=a\rho_{xx}^{\gamma}$. In order to distinguish the various contributions to the AHE mechanism, the $\rho_{AH}\sim\rho_{xx}$ relations of Mn_4N films with different thicknesses in a log–log scale are shown in Fig. 4(a). The $\rho_{AH}\sim\rho_{xx}$ curves could be fitted to a series of straight lines with slopes γ below 100 K, yet the ρ_{AH} deviates from the linear dependence at higher temperature. The scaling exponent γ shows a strong dependence on film thickness. Note that γ is larger than 2 in all the Mn_4N films. Generally, the scaling exponents γ of heterogeneous ferromagnetic systems are larger than 2, such as $\gamma=2.6$ of Fe/Cr multilayer and $\gamma=3.7$ of Co–Ag granular films.[43,44] Moreover, the interfacial scattering dominated AHE could also lead to a large γ.[45]

The anomalous Hall conductivity σ_{AH} versus σ_{xx} of Mn_4N films with different thicknesses in a log-log scale is displayed in Fig. 4(b), which implies that the σ_{xx} falls into the dirty regime. The fitted exponent γ is 1.52 at 300 K. However, the data points are dispersed below 50 K, which indicates that the AHE in Mn_4N films cannot be fitted by the scaling law of $\sigma_{AH}=A\sigma_{xx}^{\gamma}+B$ at low temperature. In order to investigate the nonlinear relationship in the high temperature induced by the temperature-dependent magnetization,[46,47] the ρ_{AH}/m versus ρ_{xx} of the 78.8 nm-thick Mn_4N film in a log-log scale is plotted in Fig. 4(c), where m is defined as $m=M_s(T)/M_s(300\ \mathrm{K})$. The data of $\log(\rho_{AH}/m)$ versus $\log\rho_{xx}$ could be well fitted in the temperature region from 5 K to 300 K. The magnetization-dependent AHE scaling law of Mn_4N films also implies that only the data below 100 K could be analyzed, where the effect of temperature-dependent magnetization on ρ_{AH} is negligible. The carriers and impurities govern the different origins of the AHE. In order to determine

whether the AHE current is dissipationless, it is necessary to factor out the carrier concentration from Hall resistivity. The dissipationless Hall resistivity confirms that the anomalous velocity origin is topological in nature and is equally valid in the Bloch and localization regimes.[48] The curve of $\log(\rho_{AH}/n_h)$ versus $\log\rho_{xx}$ at 5 K is displayed in Fig. 4(d) to investigate the dependence of ρ_{AH} on n_h. The dissipationless ρ_{AH} satisfies the relationship of $(\rho_{AH}/n_h) \propto \rho_{xx}^2$; $\alpha = 3.44$ at 5 K is obtained by linear fitting, which indicates that the ρ_{AH} of Mn_4N films is scattering-dependent.

Note that the scaling exponent γ is larger than 2 in all the films, hence other scaling laws are used to further analyze the AHE mechanism. In order to exclude the contribution of phonons to skew scattering, a proper scaling of $\rho_{AH}=\alpha\rho_{xx0}+b\rho_{xx}^2$ was proposed.[49,50] The ρ_{xx0} is residual resistivity, which represents the impurity or defects scattering in the film. The scaling constant α is considered to be from skew scattering contributions, while the constant b represents the contributions from side-jump and intrinsic mechanism. In the previous report, the scaling of $\rho_{AH} = \alpha\rho_{xx0}+b\rho_{xx}^2$ shows an excellent agreement with the experimental data.[30] Here, consider the skew scattering contributions in the conventional scaling of $\rho_{AH} = a\rho_{xx}^{\gamma}$, the differences between phonons and impurities or defects could result in the scaling exponent $\gamma > 2$. Therefore, the revised scaling of $\rho_{AH} = \alpha\rho_{xx0}+b\rho_{xx}^{n}$ was first used to separate out the temperature-independent ρ_{xx0} from different contributions. Figure 4(e) shows the scaling fit well for the Mn_4N films with different thicknesses, which confirms the difference between contributions from phonons and impurities. According to the fitting results, the scaling exponents vary from 1.61 to 2.67, indicating that the thickness-dependent ρ_{xx0} leads to the scaling exponent larger than 2. Note that the scaling exponent $n < 2$ has also been observed, the deviation of scaling exponent from 2 may be associated with the thermal disorder from a relatively skew scattering contribution.[51] Furthermore, in order to clarify the effect of impurity scattering on AHE, the $\log\rho_{AH}$–$\log\rho_{xx}$ curve at 5 K with different thicknesses is shown in Fig. 4(f). The slope value $n = 2.20$ is obtained by linear fitting, indicating that another extrinsic contribution exists besides the skew scattering.[52]

Based on the different contributions from extrinsic and intrinsic mechanisms of AHE, the relationship between ρ_{AH} and ρ_{xx} is also fitted by $\rho_{AH} = \alpha\rho_{xx0}+\beta\rho_{xx0}^2+b\rho_{xx}^2$ to further clarify the dominant mechanism in Mn_4N films.[49] The parameters of α, β and b correspond to the skew scattering, side jump and intrinsic contributions,[25,53–55] respectively. The (ρ_{AH}/ρ_{xx})–ρ_{xx} curve of Mn_4N films with different thicknesses at 5 K is displayed in Fig. 4(g). The converted equation $\rho_{AH0}/\rho_{xx0} = \alpha+(\beta+b)\rho_{xx0}$ was used to linear fitting, where the parameters $\alpha = 7.16\times10^{-5}$ and $\beta+b = 1.78\times10^{-5}$ S/cm could be obtained by the intercept and slope, respectively. As is shown in Fig. 4(h), the ρ_{AH}–ρ_{xx}^2 curves below 100 K are fitted by the scaling of $\rho_{AH} = C+b\rho_{xx}^2$ with C being constant. The proper scaling relation also shows good agreement with the data points. The intrinsic contribution b could be obtained by the slope of fitted lines, which is shown in the inset of Fig. 4(h). Note that the b is not a constant but varies with the film thicknesses, which suggests that the intrinsic ρ_{AH} exhibits strong scattering dependence. Furthermore, the σ_{AH}–σ_{xx}^2 curves below 100 K could be fitted by the formula $\sigma_{AH} = -(\alpha\sigma_{xx0}^{-1}+\beta\sigma_{xx0}^{-2})\sigma_{xx}^2-b$, the intrinsic contribution b is consistent with the values obtained by the ρ_{AH}–ρ_{xx}^2 curves. The side jump contribution β could be obtained by subtracting the intrinsic contribution b, which also varies with the film thicknesses and shows dependence on ρ_{xx0}.[56] Therefore, the dominant mechanism in the Mn_4N films is related to the competition among skew scattering, side jump and the intrinsic mechanisms.

4. Conclusions

In summary, the antiperovskite-type epitaxial Mn_4N films with different thicknesses have been deposited on MgO (001) substrates. The Hall resistivity is negative at positive magnetic field and shows a hysteresis behavior. Different scaling laws are used to distinguish the various contributions of AHE mechanisms. The deviation of the conventional scaling relation at high temperature is due to the influence of temperature-dependent magnetization. The anomalous Hall conductivity is scattering-dependent in Mn_4N films. The scaling exponent γ larger than 2 for the $\rho_{AH} \propto \rho_{xx}^{\gamma}$ in Mn_4N films with different thicknesses is the result of the contribution from ρ_{xx0}. The contributions from extrinsic and intrinsic AHE mechanisms are investigated by the proper scaling. The dominant mechanism of AHE in Mn_4N films is related to the competition among skew scattering, side jump and the intrinsic mechanisms.

Acknowledgement

This work was supported by the National Natural Science Foundation of China (Grant Nos. 51871161 and 52071233).

References

[1] Khvalkovskiy V, Apalkov D, Watts S, Chepulskii R, Beach R S, Ong A, Tang X, Driskill-Smith A, Butler W H and Visscher P B 2013 *J. Phys. D: Appl. Phys.* **46** 074001
[2] Jabeur K, Pendina G D, Bernard-Granger F and Prenat G 2014 *IEEE Electron Device Lett.* **35** 408
[3] Prenat G, Jabeur K, Vanhauwaert P, Pendina G D, Oboril F, Bishnoi R, Ebrahimi M, Lamard N, Boulle O and Garello K 2016 *IEEE Trans. Multi-Scale Comput. Syst.* **2** 49
[4] Chernyshov A, Overby M, Liu X, Furdyna J K, Lyanda-Geller Y and Rokhinson L P 2009 *Nat. Phys.* **5** 656
[5] Wadley P, Howells B, Železný J, Andrews C, Hills V, Campion R P, Novák V, Olejník K, Maccherozzi F and Dhesi S 2016 *Science* **351** 587
[6] Mi W B, Guo Z B, Feng X P and Bai H L 2013 *Acta Mater.* **61** 6387
[7] Meinert M 2016 *J. Phys.: Condens. Matter* **28** 056006

[8] Takei W J, Heikes R R and Shirane G 1962 *Phys. Rev.* **125** 1893
[9] Takei W J and Shirane G 1960 *Phys. Rev.* **119** 122
[10] Suzuki K, Yamaguchi Y, Kaneko T, Yoshida H, Obi Y, Fujimori H and Morita H 2001 *J. Phys. Soc. Jpn.* **70** 1084
[11] Eddine M N and Bertaut E F 1977 *Solid State Commun.* **23** 147
[12] Narahara A, Ito K, Suemasu T, Takahashi Y K, Ranajikanth and Hono K 2009 *Appl. Phys. Lett.* **94** 202502
[13] Ito K, Okamoto K, Harada K, Sanai T, Toko K, Ueda S, Imai Y, Okuda T, Miyamoto K, Kimura A and Sumasu T 2012 *J. Appl. Phys.* **112** 013911
[14] Yamada, K Oomaru K, Nakamura S, Sato T and Nakatani Y 2015 *Appl. Phys. Lett.* **106** 042402
[15] Ching K M, Chang W D, Chin T S and Duh J G 1994 *J. Appl. Phys.* **76** 6582
[16] Yasutomi Y, Ito K, Sanai T, Toko K and Suemasu T 2014 *J. Appl. Phys.* **115** 17A935
[17] Gushi T, Vila L, Fruchart O, Marty A, Pizzini S, Vogel J, Takata F, Anzai A, Toko K, Suemasu T and Attané J P 2018 *Jpn. J. Appl. Phys.* **57** 120310
[18] Gushi T, Klug M J, Garcia J P, Ghosh S, Attané J P, Okuno H, Fruchart O, Vogel J, Suemasu T, Pizzini S and Vila L 2019 *Nano Lett.* **19** 8716
[19] Ghosh S, Komori T, Hallal A, Garcia J P, Gushi T, Hirose T, Mitarai H, Okuno H, Vogel J, Chshiev M, Attané J P, Vila L, Suemasu T and Pizzini S 2021 *Nano Lett.* **21** 2580
[20] Nagaosa N, Sinova J, Onoda S, MacDonald A H and Ong N P 2010 *Rev. Mod. Phys.* **82** 1539
[21] Dery H, Song Y, Li P and Zûtić I 2011 *Appl. Phys. Lett.* **99** 082502
[22] Jansen R 2012 *Nat. Mater.* **11** 400
[23] Inoue J and Ohno H 2005 *Science* **309** 2004
[24] Fert A 1973 *J. Phys. F Met. Phys.* **3** 2126
[25] Berger L 1970 *Phys. Rev. B* **2** 4559
[26] Karplus R and Luttinger J M 1954 *Phys. Rev.* **95** 1154
[27] Sangiao S, Morellon L, Simon G, Teresa J M D, Pardo J A, Arbio J and Ibarra M R 2009 *Phys. Rev. B* **79** 014431
[28] Fernández-Pacheco A, Teresa J M D, Orna J, Morellon L, Algarabel P A, Pardo J A and Ibarra M R 2008 *Phys. Rev. B* **77** 100403
[29] Li D, Hu P, Meng M, Li H, Wu S and Li S 2018 *Mater. Res. Bull.* **101** 162
[30] Meng M, Wu S X, Ren L Z, Zhou W Q, Wang Y J, Wang G L and Li S W 2015 *Appl. Phys. Lett.* **106** 032407
[31] Kabara K, Tsunoda M and Kokado S 2017 *AIP Adv.* **7** 056416
[32] Shen X, Chikamatsu A, Shigematsu K, Hirose Y, Fukumura T and Hasegawa T 2014 *Appl. Phys. Lett.* **105** 072410
[33] Mi W B, Guo L, Jiang E Y, Li Z Q, Wu P and Bai H L 2003 *J. Phys. D: Appl. Phys.* **36** 2393
[34] Zhang Y, Mi W B, Wang X C and Zhang X X 2015 *Phys. Chem. Chem. Phys.* **17** 15435
[35] Onoda S, Sugimoto N and Nagaosa N 2008 *Phys. Rev. B* **77** 165103
[36] Zhao K, Hajiri T, Chen H, Miki R, Asano H and Gegenwart P 2019 *Phys. Rev. B* **100** 045109
[37] Wang L, Feng Q, Lee H G, Ko E K, Lu Q and Noh T W 2020 *Nano Lett.* **20** 2468
[38] Yasuda K, Wakatsuki R, Morimoto T, Yoshimi R, Tsukazaki A, Takahashi K S, Ezawa M, Kawasaki M, Nagaosa N and Tokura Y 2016 *Nat. Phys.* **12** 555
[39] Liu N, Teng J and Li Y 2018 *Nat. Commun.* **9** 1282
[40] Seemann K M, Mokrousov Y, Aziz A, Miguel J, Kronast F, Kuch W, Blamire M G, Hindmarch A T, Hickey B J, Souza I and Marrows C H 2010 *Phys. Rev. Lett.* **104** 076402
[41] Kim T W and Gambino R J 2000 *J. Appl. Phys.* **87** 1869
[42] Jin Y, Valloppilly S, Kharel P, Waybright J, Lukashev P, Li X Z and Sellmyer D J 2018 *J. Appl. Phys.* **124** 103903
[43] Song S N, Sellers C and Ketterson J B 1991 *Appl. Phys. Lett.* **59** 479
[44] Xiong P, Xiao G and Wang J Q 1992 *Phys. Rev. Lett.* **69** 3220
[45] Guo Z B, Mi W B, Aboljadayel R O, Zhang B, Zhang Q, Barba P G, Manchon A and Zhang X X 2012 *Phys. Rev. B* **86** 104433
[46] Zhang Q, Li P, Wen Y, He X, Zhao Y L, Zhang J L and Zhang X X 2017 *J. Phys. D: Appl. Phys.* **50** 235002
[47] Zhang Q, Wen Y, Zhao Y L, Li P, He X, Zhang J L, He Y, Peng Y, Yu R H and Zhang X X 2017 *J. Phys.: Condens. Matter* **29** 415802
[48] Lee W L, Watauchi S, Miller V L, Cava R J and Ong N P 2004 *Science* **303** 1647
[49] Tian Y, Ye L and Jin X 2009 *Phys. Rev. Lett.* **103** 087206
[50] Hou D, Li Y, Wei D, Tian D, Wu L and Jin X 2012 *J. Phys.: Condens. Matter* **24** 482001
[51] Gerber A, Milner A, Finkler A, Karpovski M, Goldsmith L, Tuaillon-Combes J, Boisron O, Mélinon P and Perez A 2004 *Phys. Rev. B* **69** 224403
[52] Yue D and Jin X 2017 *J. Phys. Soc. Jpn.* **86** 011006
[53] Fert A and Friederich A 1976 *Phys. Rev. B* **13** 397
[54] Smit J 1955 *Physica* **21** 877
[55] Smit J 1958 *Physica* **24** 39
[56] Zhang Q, Zheng D X, Wen Y, Zhao Y L, Mi W B, Manchon A, Boulle O and Zhang X X 2020 *Phys. Rev. B* **101** 134412